





Lipofuscin labeling through biorthogonal strain-promoted azide-alkyne cycloaddition for the detection of senescent cells

Beatriz Lozano-Torres^{1,2,3} , Juan F. Blandez^{1,3,4} , Alba García-Fernández^{1,2,3} , Félix Sancenón^{1,2,3,4}  and Ramón Martínez-Máñez^{1,2,3,4} 

1 Instituto Interuniversitario de Investigación de Reconocimiento Molecular y Desarrollo Tecnológico (IDM), Universitat Politècnica de València, Universitat de València, Spain

2 Unidad Mixta UPV-CIPF de Investigación en Mecanismos de Enfermedades y Nanomedicina, Centro de Investigación Príncipe Felipe, Universitat Politècnica de València, Spain

3 CIBER de Bioingeniería, Biomateriales y Nanomedicina (CIBER-BBN), Madrid, Spain

4 Unidad Mixta de Investigación en Nanomedicina y Sensores, IIS La Fe, Universitat Politècnica de València, Valencia, Spain

Keywords

alkyne-azide cycloaddition; cellular senescence; detection; lipofuscin; Sudan Black B

Correspondence

R. Martínez-Máñez and J. F. Blandez, Instituto Interuniversitario de Investigación de Reconocimiento Molecular y Desarrollo Tecnológico (IDM), Universitat Politècnica de València, Universitat de València. Camino de Vera s/n, 46022-Valencia, Spain
 Tel: 963877343
 E-mails: rmaez@qim.upv.es (R.M.-M.); juablaba@upvnet.upv.es (J.F.B.B.)

A new method for senescent cell detection is described, which is based on lipofuscin labeling with a fluorescent reporter through a biorthogonal strain-promoted azide-alkyne cycloaddition. The sensing protocol involves a first step where the interaction of lipofuscin with a Sudan Black B derivative containing an azide moiety (**SBB-N₃**) is carried out. In the final step, the azide moiety reacts with a fluorophore containing a cyclooctene ring (**BODIPY**). The efficacy of this two-step protocol is assessed in senescent melanoma SK-MEL-103 cells, senescent triple-negative breast cancer MDA-MB-231 cells and senescent WI-38 fibroblasts. In all cases, a clear fluorescence pattern was observed in senescent cells, compared to proliferative cells, only when the **SBB-N₃-BODIPY** probe was formed. Our results provide an alternative tool for the detection of senescent cells, based on an *in situ* bio-orthogonal reaction for lipofuscin labeling.

(Received 15 September 2021, revised 31 March 2022, accepted 6 May 2022)

doi:10.1111/febs.16477

Introduction

Cellular senescence is a biological process triggered in response to stress or damage [1]. This process has a relevant physiological role during development and promotes tissue regeneration. However, the accumulation of senescent cells can produce inflammation, fibrosis, tissue aging or tumorigenesis, amongst other diseases [1–5]. Considering the significance of cellular senescence in age-related disorders and carcinogenesis, there is a growing interest in

the detection and elimination of senescent cells [6–10]. Senolysis (i.e. therapies against senescent cells) has been reported to induce remarkable therapeutic effects on multiple diseases in mice, thus considering the elimination of senescent cells as a promising strategy to treat aging-related diseases [5,11,12].

By contrast, the detection of senescent cells is a field in rapid and continuous development and, as a result

Abbreviations

ATR-FTIR, attenuated total reflectance Fourier transform infrared; DMEM, Dulbecco's modified Eagle's medium; DMF, dimethylformamide; PBS, phosphate buffer saline; SA- β -Gal, senescence-associated β -galactosidase; SBB, Sudan Black B; SPAAC, strain-promoted alkyne-azide cycloaddition.

of the lack of a unique signature for senescence, the possibility having a collection of chemical tools with the ability to detect senescent cells is of great concern. One of the most widely used markers to detect cellular senescence is the overexpression of lysosomal β -galactosidase, also known as senescence-associated β -galactosidase (SA- β -Gal), and the detection of SA- β -Gal activity using chromo-fluorogenic probes has become a simple and popular procedure in laboratories for detecting senescence [13–16]. Most of these reported probes are composed of a galactose unit covalently linked, through N- or O-glycosidic bonds with a selected fluorophore. Nevertheless, these probes show certain limitations, such as, for example, the fact that cells overexpressing β -galactosidase are not always senescent cells [17,18].

Furthermore, lipofuscin, known as the ‘age pigment’, is a non-degradable aggregate of oxidized lipids, covalently cross-linked proteins, oligosaccharides and transition metals that accumulate within lysosomes in aged post-mitotic cells [19]. Lipofuscin accumulation is also observed in senescent cells, thus establishing it as an additional biomarker to detect senescence [20]. However, when compared with sensors for the SA- β -Gal detection, the development of molecular probes for lipofuscin labeling has been much less explored. Lipofuscin is traditionally histochemically detected by reaction with oil-soluble dyes, such as Sudan Black B (SBB), with this method being well known in the pathological community [21–23]. However, these classical histological protocols present several technical drawbacks such as (a) the need for high magnification for light microscopy; (b) require high experience as a pathologist; and (c) SBB dye contains numerous impurities that precluded the unambiguous readout of the analysis because of ‘background dirt’ [19].

To overcome the above-mentioned drawbacks, Gorgoulis *et al.* [24] improved the classical protocol using an avidin-biotin conjugation. In this protocol, the samples are incubated with an SBB-biotin conjugate, which binds with lipofuscin. In a second step, an anti-biotin antibody containing a peroxidase-conjugated polymeric backbone is added. Afterwards, the addition of 3,3'-diaminobenzidine (a peroxidase substrate) induces the appearance of a blue–black product (as a result of the enzyme-catalyzed oxidation of 3,3'-diaminobenzidine) indicating the presence of lipofuscin. However, this method requires the previous blocking of endogenous hydrogen peroxidase, and it is reported that an inefficient inactivation of the peroxidase enzyme might cause false positives in the staining protocol.

In this scenario, we envisioned the possibility to employ bio-orthogonal reactions for lipofuscin labeling

that could operate in the complex cellular matrix without the need of previously blocking cellular endogenous components for the detection of lipofuscin. Bio-orthogonal reactions are employed for the selective formation of covalent bonds in biological media and have been widely used in drug design, biomolecule labeling and *in vivo* imaging. Staudinger ligation reactions, inverse electron demand Diels–Alder reactions, palladium catalyzed cross-coupling reactions, ruthenium catalyzed cross-metathesis reactions, Cu(I) catalyzed 1,3-dipolar azide-alkyne cycloadditions and strain-promoted alkyne-azide cycloaddition (SPAAC) are the most frequently used [25]. Inside the realm of bio-orthogonal reactions, click reactions are fast, exquisitely specific and high-yielding reactions that are carried out between two mutually reactive molecular counterparts and that occur with negligible perturbation of the native activities of biomolecules [26–29]. One of the most popular click chemistry reactions is the Cu(I) catalyzed 1,3-dipolar azide-alkyne cycloaddition, which generates a stable 1,2,3-triazole linkage [30–34]. For biological applications, and to overcome the cytotoxicity of Cu(I), click reactions employ internal cyclooctynes instead of linear alkynes, which allows the click reaction to occur in biological settings without the presence of Cu(I), with this type of reaction named as SPAAC [35–37].

Based on the aforementioned and in our interest in the synthesis of molecular probes and materials for the detection of senescent cells [5,6,13–16], in the present study, we report a new method for lipofuscin labeling using a SPAAC reaction between an SBB derivative, modified with an azide group (SBB-N₃) and a BODIPY fluorophore functionalized with a strained cyclooctyne ring (BODIPY). The efficacy of this two-steps protocol is assessed in different senescent cellular models. A significant emissive signal from BODIPY is observed in senescent cells in comparison with proliferative cells because of the formation of the SBB-N₃-BODIPY probe anchored to lipofuscin.

Results and discussion

Synthesis, characterization and sensing mechanism

Figure 1A shows the proposed sensing protocol for the fluorescence detection of lipofuscin. In the first step, SBB-N₃ is internalized in senescent cells and aggregates to lipofuscin. Then, in a second step, cells are treated with BODIPY, with the SPAAC reaction taking place between the azide group of SBB-N₃ (located in the lipofuscin) and the cyclooctyne ring in BODIPY, resulting

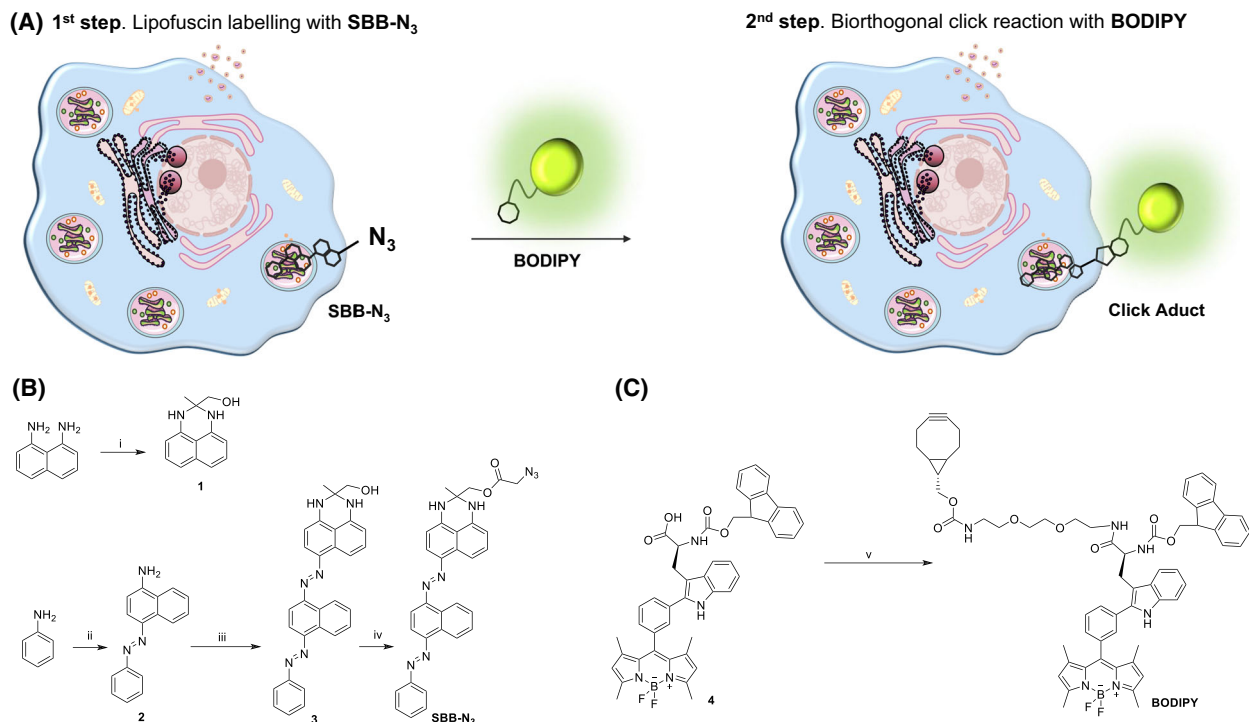


Fig. 1. (A) Proposed mechanism for new senescent cell detection protocol through lipofuscin labeling with a Sudan Black B derivative containing an azide moiety (**SBB-N₃**) and subsequent reaction with a fluorophore containing a strained cyclooctyne ring (**BODIPY**) by a biorthogonal SPAAC reaction. (B) Synthetic procedure followed to obtain **SBB-N₃**: i: hydroxyacetone, EtOH, 3 h, 65 °C; ii: 1-aminonaphthalene, NaNO₂, H₂O/HCl (10 : 7), 10 h, RT; iii: **1** + **2**, NaNO₂, DMF/H₂O/HCl (2 : 3 : 0.6), 90 min, RT, to obtain **3**; iv: **3** + 2-azidoacetic acid, *N,N'*-dicyclohexylcarbodiimide, 4-dimethylaminopyridine, anhydrous DCM, 5 days, RT]. (C) Synthetic protocol used to prepare the cyclooctyne-containing BODIPY fluorophore (v: *N*-[(1*R*,8*S*,9*S*)-bicyclo[6.1.0]non-4-yn-9-yl)methylloxycarbonyl]-1,8-diamino-3,6-dioxaoctane); **4**, 1,1,3,3-tetramethyl-2-[2-oxopyridin-1(2H)-yl]isouronium hexafluorophosphate, *N,N*-diisopropylethylamine, anhydrous DMF, RT, 24 h.

in the labeling of lipofuscin and allowing its visualization via fluorescence. The synthetic procedures used to prepare **SBB-N₃** [24], and **BODIPY** are depicted in Fig. 1B,C. Briefly, the substituted perimidine, (2-methyl-2,3-dihydro-1H-perimidin-2-yl)methanol (**1**), was obtained through a condensation reaction between 1,8-diaminonaphthalene and hydroxyacetone. Simultaneously, (*E*)-4-(phenyldiazenyl)naphthalen-1-amine (**2**) was obtained using a diazotization reaction between aniline and 1-naphthylamine. The diazotization coupling reaction between **1** and **2** followed by the esterification of the hydroxyl moiety of condensation product with azidoacetic acid yielded **SBB-N₃**. On the other hand, a commercially available fluorophore bearing a carboxylic acid moiety (**4**) was reacted with the strained cycloalkyne **5**, yielding **BODIPY**. The obtained compounds were fully characterized by ¹H-NMR and ¹³C-NMR, (Figs S1–S5). The formation of the click adduct after the SPAAC reaction between **SBB-N₃** and **BODIPY** was analyzed using attenuated total reflectance Fourier transform infrared (ATR-FTIR) spectroscopy and HPLC-MS measurements. The ATR-FTIR spectra

of **SBB-N₃** and **BODIPY** reagents and of the click reaction adduct (Fig. 2A, i and ii) showed the disappearance of the stretching band of the azide moiety of **SBB-N₃** at 2101.7 cm⁻¹ and the appearance of a weak band at 1740.1 cm⁻¹ ascribed to the formed 1,2,3-triazole heterocycle. In addition, Fig. 2B shows the HPLC-MS chromatograms of **BODIPY** (*t_R* = 9.55 min), **SBB-N₃** (*t_R* = 8.90 min) and the SPAAC cycloaddition reaction (only one peak with *t_R* = 13.06 min). Selected-ion monitoring chromatogram of the click reaction adduct peak at 13.06 min showed a *m/z* value of 1610.71, which correlated with the theoretical value of molecular ion C₉₃H₉₀BF₂N₁₅O₉ (Fig. 2C and Fig. S6).

***In vitro* validation of the SPAAC reaction in different senescent cellular models**

In a first step, before applying **SBB-N₃** + **BODIPY** labeling in cellular experiments, we tested the possible cytotoxicity of **SBB-N₃**, **BODIPY** compounds and the combination of **SBB-N₃** + **BODIPY** in proliferating and senescent SK-Mel-103 (human melanoma) cells.

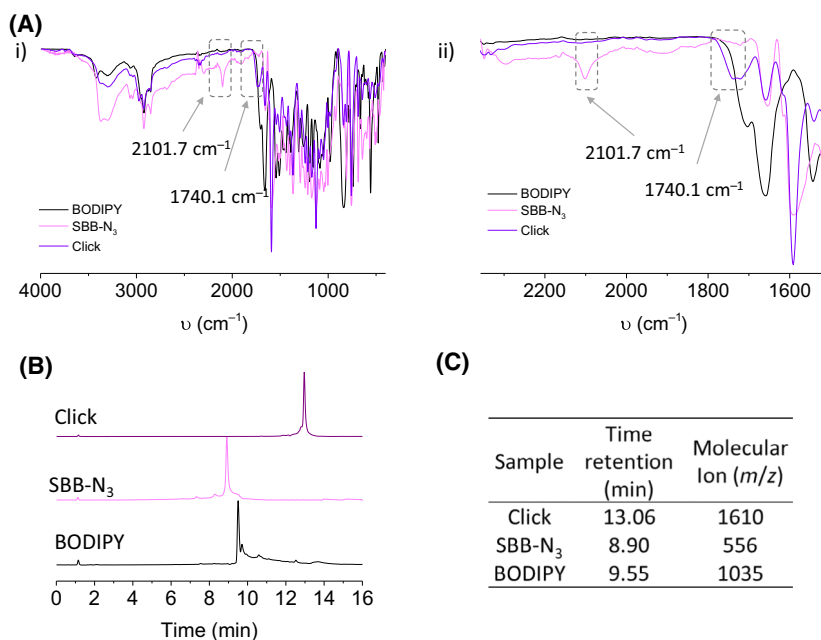


Fig. 2. (A, i) ATR-FTIR spectrum of **BODIPY**, **SBB-N₃**, and the product after click reaction. (A, ii) ATR-FTIR spectrum between 2400 and 1500 cm^{-1} showing the disappearance of the stretching band of the azide moiety of **SBB-N₃** at 2101.7 cm^{-1} and the appearance of a weak band at 1740.1 cm^{-1} ascribed to the formed 1,2,3-triazole heterocycle. (B) HPLC-MS studies of the click reaction between **SBB-N₃** and **BODIPY** using the selected-ion monitoring technique. The chromatograms show the appearance of the click adduct (**SBB-N₃-BODIPY**) as a unique peak at 13.06 min after 5 h. The signal at 9.55 min corresponds to **BODIPY**, whereas the signal at 8.90 min is ascribed to **SBB-N₃**. (C) Values of the molecular ions as *m/z* corresponding to the above mentioned retention times.

The viability assays (Fig. S7) showed that **SBB-N₃** and **BODIPY** are not toxic after 48 h even at high concentrations. Furthermore, after the combined treatment with both compounds, no significant differences were observed in cell viability, compared to untreated cells, up to 2.5 $\mu\text{g}\cdot\text{mL}^{-1}$ for **SBB-N₃** and 5 μM **BODIPY**, respectively. We selected this dose range for further cellular assays. Senescence in SK-Mel-103 cells was induced by incubating the cells with the CDK4/6 inhibitor palbociclib (5 μM) for 1 week. As expected, an increase in cell size and the number of intracellular vesicles was observed and the overexpression of the β -galactosidase enzyme was confirmed by X-Gal cellular staining assay (Fig. 3A, i and ii). Moreover, the staining of lipofuscin granules was confirmed in senescent cells after **SBB-N₃** treatment. For this purpose, proliferating and palbociclib-treated cells were incubated with a solution containing **SBB-N₃** (3.2 $\mu\text{g}\cdot\text{mL}^{-1}$) in Dulbecco's modified Eagle's medium (DMEM) (0.1% dimethylsulfoxide) for 2 h. Then, cells were washed and analyzed by light microscopy. The positive lipofuscin staining was confirmed in palbociclib-treated SK-Mel-103 cells in which a brown-black granule pattern was observed. This staining was not observed in proliferating SK-Mel-103 cells (Fig. 3A, iii and iv).

Then, the labeling ability of **SBB-N₃ + BODIPY**, through the SPAAC reaction, was assessed in senescent cells. For this purpose, a two-step procedure was carried out and fluorescence was analyzed by confocal microscopy or flow cytometry. First, control and senescent SK-Mel-103 cells were incubated with a

solution containing **SBB-N₃** (3.2 $\mu\text{g}\cdot\text{mL}^{-1}$ in DMEM, 0.1% dimethylsulfoxide) for 2 h to incorporate the azide moieties into lipofuscin. Then, cells were washed and treated with **BODIPY** (5 μM) for 1 h to allow the specific fluorescence staining of lipofuscin via the SPAAC reaction. Finally, cells were washed and analyzed by confocal microscopy or by flow cytometry using 488 nm as the excitation wavelength. Figure 3B shows a representative image of both proliferative and senescent SK-Mel-103 after **SBB-N₃ + BODIPY** treatment. Senescent cells treated with **SBB-N₃** and **BODIPY** showed a clear bright green emission compared to control cells. The observed fluorescence signal was localized in medium-to-large-sized perinuclear structures or small granules distributed in the cytoplasm, which is consistent with lipofuscin staining. Control and senescent cells not treated with **SBB-N₃ + BODIPY** did not show significant fluorescence at working conditions. Confocal images were analyzed and quantified using IMAGEJ (NIH, Bethesda, MD, USA), corroborating an approximately 2.9-fold higher emission intensity in senescent cells compared to control cells (Fig. 3C). Finally, flow cytometry quantification revealed that approximately 69% of senescent cells treated with **SBB-N₃ + BODIPY** were positive to the staining compared to proliferating cells also treated with both products (approximately 7%) (Fig. 3D, vii and viii, and Fig. S8). Autofluorescence from control and senescent cells was also discarded (Fig. 3D, v and vi) by adjusting laser conditions to avoid autofluorescence from senescent cells. These results are consistent

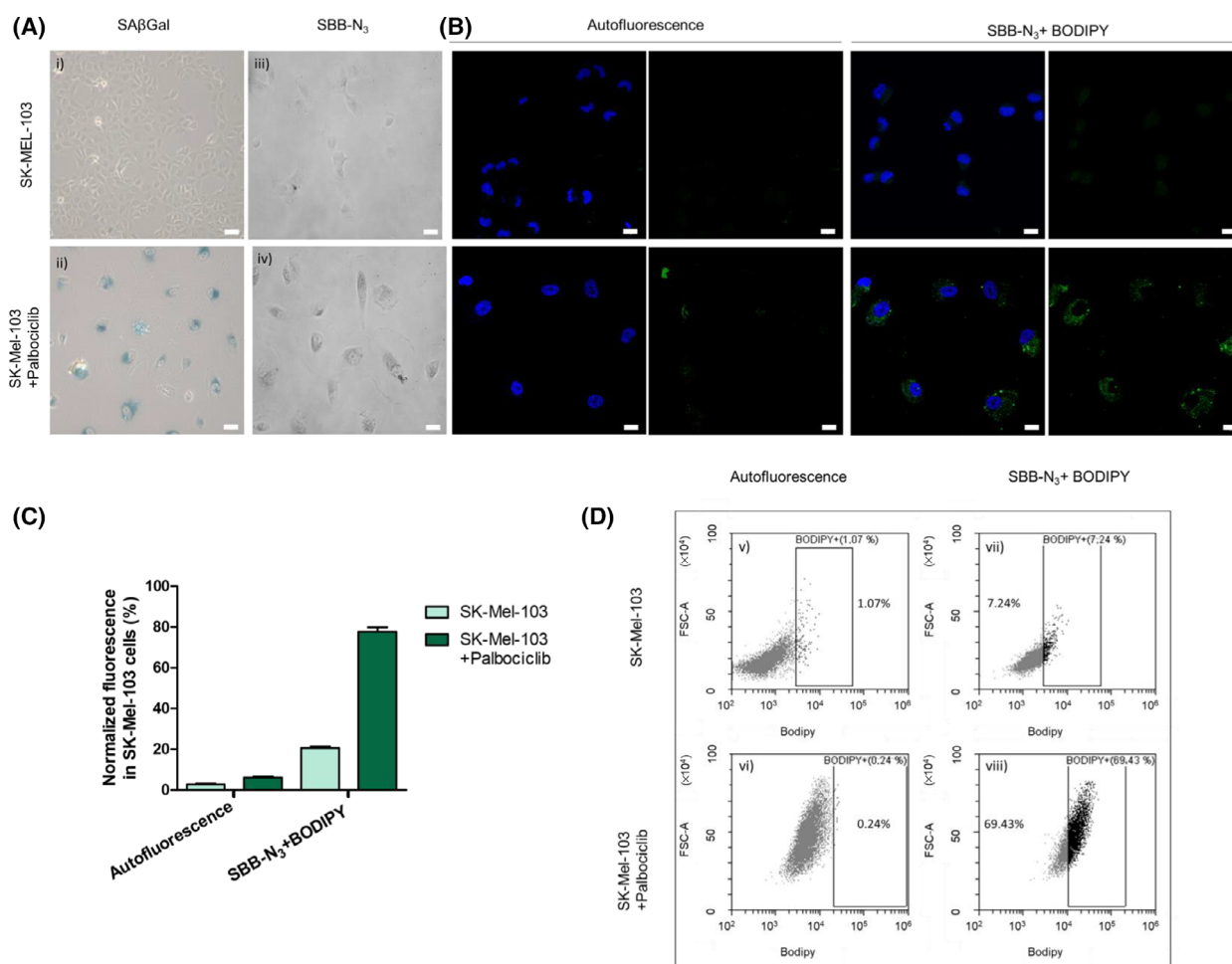


Fig. 3. (A) Conventional X-Gal assay for detection of SA- β Gal expression in control (i) and palbociclib-treated (ii) SK-Mel-103 cells. **SBB-N₃** staining for lipofuscin detection in (iii) control and (iv) palbociclib-treated SK-Mel-103 cells. Scale bar = 20 μ m. (B) Confocal images of control SK-Mel-103 cells in the absence or after **SBB-N₃ + BODIPY** treatment. First, cells were incubated with 3.2 mg·mL⁻¹ **SBB-N₃** (2 h, 37 °C, 20% O₂, 5% CO₂) and washed 3 \times with DMEM, then cells were treated with 5 μ M **BODIPY** (1 h, 37 °C, 20% O₂, 5% CO₂). SK-Mel-103 treated with palbociclib in the absence or after **SBB-N₃ + BODIPY** treatment showing the dotted pattern ascribed to lipofuscin granules. Scale bar = 20 μ m. (C) Quantification of normalized fluorescence observed in the confocal images in SK-Mel-103 cells. (D) Flow cytometry quantification of the percentage of stained SK-Mel-103 cells in the absence (v) or after (vii) **SBB-N₃ + BODIPY** treatment and palbociclib-treated SK-Mel-103 cells in the absence (vi) or after (viii) of **SBB-N₃ + BODIPY** treatment. Cells were incubated with 3.2 μ g·mL⁻¹ **SBB-N₃** (2 h, 37 °C, 20% O₂, 5% CO₂) washed 3 \times with DMEM, and treated with 5 μ M **BODIPY** (1 h, 37 °C, 20% O₂, 5% CO₂). The results are expressed as the mean \pm SD of three independent studies ($n = 3$).

with the lower levels of lipofuscin in proliferating cells compared to the characteristic higher expression in senescent cells [15]. To certify the ability of **SBB-N₃ + BODIPY** to stain senescent cells, proliferative and senescent cells were also treated with **SBB-N₃** or **BODIPY** as a control. In the case of control cells, any effect was observed after **SBB-N₃**. However, in the case of senescent cells, considering the laser conditions established to discard any possible interference between autofluorescence and probes, only some autofluorescence signals were observed, which were completely masked after **SBB-N₃** treatment (Fig. S9).

When we treated control or senescent cells with **BODIPY**, a high fluorescence signal was detected in both proliferative and senescent cells, thus confirming the non-specific staining (Fig. S9). Therefore, a clear fluorescence pattern was observed in senescent cells compared to proliferative cells only when **SBB-N₃-BODIPY** was formed.

In addition, the activity of the **SBB-N₃-BODIPY** was evaluated in other senescent cellular models, including triple-negative breast cancer MDA-MB-231 cells, as another cancer model, and WI-38 fibroblasts derived from lungs as non-cancerous cells. As

expected, after treatment with palbociclib (5 μM) for 1 week, an increase in cell size and the number of intracellular vesicles was observed, as well as the overexpression of the β -galactosidase enzyme, confirmed by a X-Gal cellular staining assay in both MDA-MB-231 and WI-38 cells (Fig. 4A,B). The possible toxicity of **SBB-N₃**, **BODIPY** or combined **SBB-N₃ + BODIPY** was discarded in proliferating and senescent cells for both MDA-MB-231 and WI-38 cell lines. No significant differences were observed in cell viability after the treatment with the compounds after 48 h, even at high concentrations, compared to untreated cells (Fig. S7). Finally, the labeling ability of **SBB-N₃ + BODIPY**, following the two-step procedure described above, was confirmed via confocal image assays. Autofluorescence from control and senescent cells was also discarded. In both cases, a significant fluorescence pattern was observed in senescent cells treated with **SBB-N₃ + BODIPY** compared to proliferative cells. The fluorescence signal was clearly localized in medium-to-large-sized perinuclear structures or small granules distributed in the cytoplasm, which is consistent with lipofuscin staining (Fig. 4A,B). Furthermore, proliferative and senescent cells were treated with **SBB-N₃** or the **BODIPY** as control in both cell lines (Figs S10 and S11), thus confirming significant fluorescence staining of senescent cells only when the complex **SBB-N₃-BODIPY** is formed. The fluorescence intensity was also quantified using IMAGEJ, showing an approximately 2.3- and 2.9-fold enhancement of emission intensity for senescent MDA-MB-231 and WI-38 cells, respectively, compared to control cells (Fig. 4C,D).

Overall, these findings confirmed the proper working of the SPAAC reaction between **SBB-N₃** and **BODIPY** for the fluorescence labeling of senescent cells.

Conclusions

In summary, in the present study, we describe a new procedure for the detection of senescent cells by lipofuscin labeling using a strain-promoted alkyne-azide bio-orthogonal cycloaddition. The procedure is based on the well-known staining of lipofuscin with **SBB** dye. The protocol first involves the interaction of the **SBB-N₃** derivative (functionalized with an azide moiety) with lipofuscin and then a reaction with **BODIPY** (containing a strained cyclooctyne ring) to give a final **SBB-N₃-BODIPY** adduct. The SPAAC reaction between **SBB-N₃** and **BODIPY** is confirmed by ATR-FTIR spectroscopy and HPLC-MS measurements. The possible toxicity of the **SBB-N₃**, **BODIPY** and **SBB-N₃ + BODIPY** probe was discarded in both

proliferating and senescent cells. The labeling ability of **SBB-N₃ + BODIPY**, through SPAAC reaction, was assessed in human melanoma SK-Mel-103 senescent cells. Flow cytometry quantification revealed that senescent cells incubated with **SBB-N₃ + BODIPY** are positive (approximately 70%) compared to proliferating cells (approximately 7%). Moreover, senescent SK-Mel-103 cells treated with **SBB-N₃ + BODIPY** show a clear bright green emission by confocal microscopy compared to control cells. Furthermore, the combination of **SBB-N₃ + BODIPY** was validated in senescent triple-negative breast cancer MDA-MB-231 cells and in senescent WI-38 fibroblasts. In both cases, a significant fluorescence pattern was only observed in senescent cells treated with **SBB-N₃ + BODIPY** compared to proliferative cells. This work provides an alternative new tool for the detection of senescent cells through lipofuscin labeling, which substantially differs from the more classical procedures based on the detection of the overexpression of lysosomal β -galactosidase activity. In addition, our staining protocol was shown to be stable, allowing monitoring of fluorescence in living cells for hours in chemotherapy-induced senescence cellular models. Further studies are being developed by us aiming to validate our findings in age-related models such as young and old primary cultures, as well as in aged animals.

Materials and methods

Materials

All chemical reagents were purchased from Sigma-Aldrich (St Louis, MO, USA). On the other hand, anhydrous solvents and phosphate-buffered saline (PBS) were purchased from Scharlab S.L. (Barcelona, Spain) and used without further purification. Palbociclib was acquired from Selleckchem (Houston, TX, USA) and DMEM and fetal bovine serum was purchased from Gibco (Waltham, MA, USA). Flat-bottom-clear 96-well plates were purchased from Promega (Madison, WI, USA). HPLC-MS was recorded with an Agilent 1620 Infinity II HPLC coupled to a mass spectrometer Agilent Ultivo equipped with a triple QTOF detector (Agilent, Santa Clara, CA, USA). Fourier-transform infrared (ATR-FTIR) spectra were recorded using a Nicolet 6700 instrument (Thermo Scientific, Waltham, MA, USA) in the range 4000–400 cm^{-1} . ^1H - and ^{13}C -NMR spectra were collected on a Bruker FT-NMR Avance 400 (Bruker, Ettlingen, Germany) spectrometer at 300 K, using tetramethylsilane as internal standard. Luminescence was collected in a VICTOR Multilabel Plate Reader (PerkinElmer, Waltham, MA, USA). Confocal fluorescence images were taken on a TCS SP8 AOBS (Leica, Wetzlar, Germany). Images were analyzed using IMAGE J.

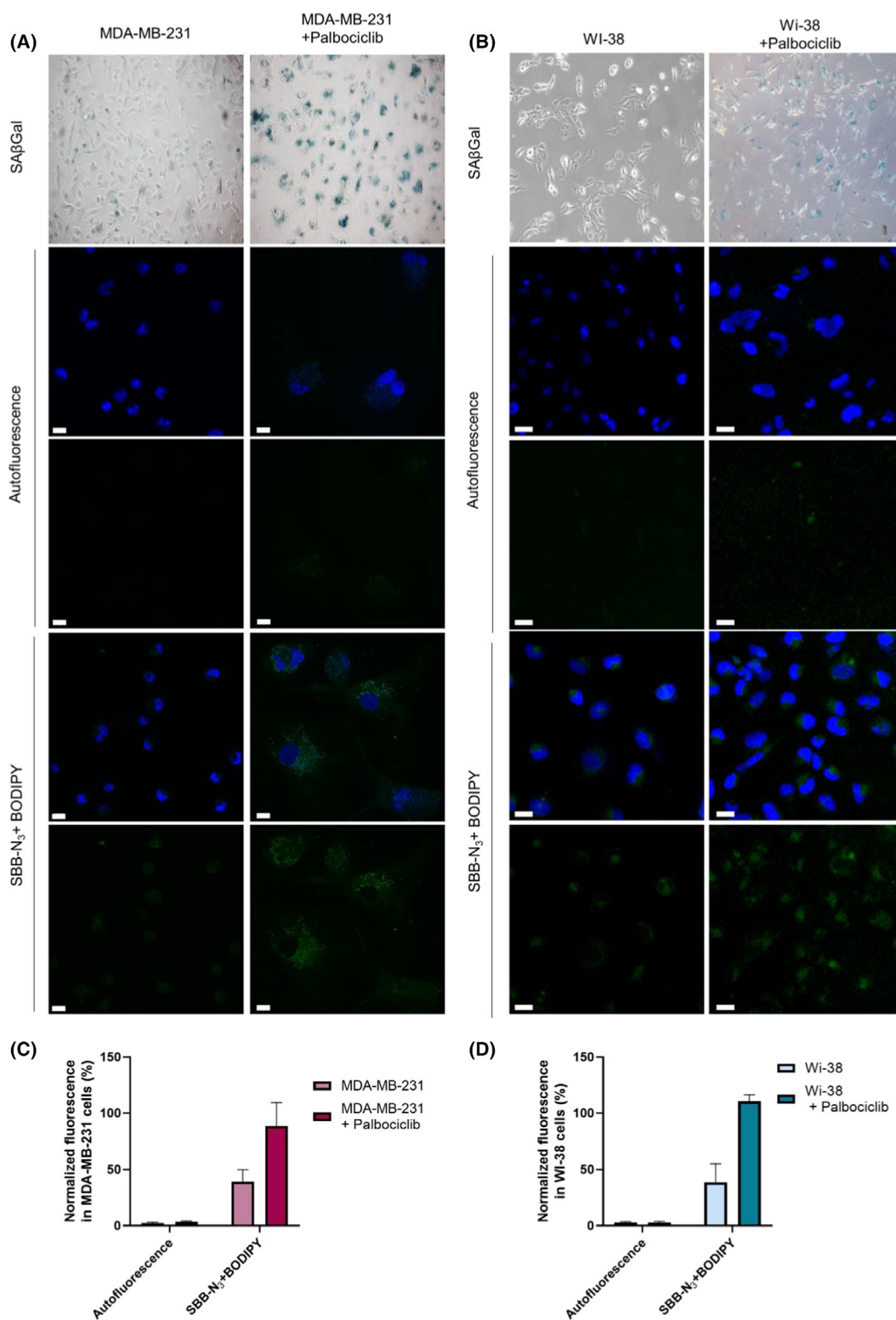


Fig. 4. (A) Proliferative and palbociclib treated MDA-MB-231 cells and (B) proliferative and palbociclib treated WI-38 cells. Up: Conventional X-Gal assay for detection of SA- β -Gal expression. Down: confocal images of proliferative and senescent cells in the absence or after **SBB-N₃ + BODIPY** treatment. Scale bar = 10 μ m. (C) Quantification of fluorescence intensity in MDA-MB-231 cells. (D) Quantification of fluorescence intensity in WI-38 cells. The results are expressed as the mean \pm SD of three independent studies ($n = 3$).

Synthesis of (2-methyl-2,3-dihydro-1H-perimidin-2-yl)methanol (**1**)

Diaminonaphthalene (1.58 g, 10 mmol) was dissolved in absolute ethanol (10 mL) and then hydroxyacetone (1.11 g, 15 mmol) was added to the solution. Mixture was heated at 75 °C under stirring. After 3 h, solvent was removed under reduced pressure, water (50 mL) was added into the residue and extracted with dichloromethane (3 × 50 mL). The organic layer was washed with brine (100 mL) and dried with sodium sulfate. Solvent was removed to obtain the pure compound (**1**) as a dark brown solid in a 91.5% yield. ¹H-NMR (400 MHz, CDCl₃) δ 7.24 (dd, *J* = 8.2, 7.3 Hz, 2H), 7.17 (dd, *J* = 8.3, 0.9 Hz, 2H), 6.52 (dd, *J* = 7.2, 1.0 Hz, 2H), 4.37 (s, 1H), 3.57 (s, 2H), 1.49 (s, 3H). ¹³C-NMR (101 MHz, CDCl₃) δ 139.55 (2C), 134.73 (1C), 127.19 (2C), 117.75 (2C), 113.22 (2C), 106.70 (1C), 67.21 (1C), 66.77 (1C), 24.89 (1C).

Synthesis of (*E*)-4-(phenyldiazenyl)naphthalen-1-amine (**2**)

Aniline (3.39 g, 36 mmol) was dissolved in a mixture of HCl : H₂O (7 : 10 mL). On the other hand, NaNO₂ (2.5 g, 37 mmol) was dissolved in water (2 mL) and added dropwise to the aniline solution at 0 °C. After 2 h, the mixture reaction was neutralized with potassium acetate until pH 6. Neutralized mixture was added dropwise to a solution of 1-aminonaphthalene (5.52 g, 38.5 mmol) in a mixture of HCl : H₂O : EtOH (3 : 100 : 12 mL) at 0 °C. The reaction mixture was stirred at room temperature. After 10 h, the reaction was neutralized with potassium acetate until pH 8–9. Product **2** was obtained, as brown dark solid, by precipitation and purification by chromatography column using dichloromethane as eluent (yield 65%). ¹H-NMR (400 MHz, CDCl₃) δ 9.06 (d, *J* = 9.3 Hz, 1H), 7.99 (dd, *J* = 5.2, 3.2 Hz, 2H), 7.93 (d, *J* = 7.9 Hz, 1H), 7.83 (d, *J* = 8.9 Hz, 1H), 7.65 (ddd, *J* = 9.3, 6.4, 1.0 Hz, 1H), 7.58–7.50 (m, 3H), 7.46–7.41 (m, 1H), 6.83 (d, *J* = 7.9 Hz, 1H), 4.61 (s, 2H). ¹³C-NMR (101 MHz, CDCl₃) δ 153.67 (1C), 146.33 (1C), 140.60 (1C), 133.30 (1C), 129.92 (1C), 129.16 (2C), 127.22 (1C), 125.51 (1C), 124.29 (1C), 122.80 (2C), 122.66 (1C), 120.73 (1C), 113.98 (1C), 109.28 (1C), 107.18 (1C).

Synthesis of (2-methyl-6-[(*E*)-4-[(*E*)-phenyldiazenyl]naphthalene-1-yl]diazenyl]-2,3-dihydro-1H-perimidin-2-yl)methanol (**3**)

(*E*)-4-(phenyldiazenyl)naphthalen-1-amine (**2**) (0.5 g, 2.02 mmol) was dissolved in dimethylformamide (DMF) : H₂O : HCl mixture (2 : 3 : 0.6 mL) and cooled at 0 °C. NaNO₂ (0.139 g, 2.02 mmol) in water (1 mL) was added dropwise to the solution of **2**. The diazonium salt formed was stirred for 2 h at 0 °C. (2-methyl-2,3-dihydro-1H-

perimidin-2-yl)methanol (**1**) (0.428 g, 2 mmol) was dissolved in ethanol (2 mL). Diazonium salt was added dropwise to the solution of **1** under vigorous stirring at 0 °C. The solution was stirred at 0 °C for 30 min and then at room temperature for 90 min. The solution was neutralized with NaHCO₃. The solid was separated by filtration and washed with cold water. The solid was purified by reverse phase column chromatography using methanol as eluent. Product **3** was obtained as purple solid (yield 85%). ¹H-NMR (400 MHz, CDCl₃) δ 9.11 (s, 1H), 9.07–9.02 (m, 1H), 8.46 (d, *J* = 8.5 Hz, 1H), 8.15 (d, *J* = 8.4 Hz, 1H), 8.09 (d, *J* = 7.4 Hz, 2H), 8.01 (dd, *J* = 20.3, 8.4 Hz, 2H), 7.76–7.69 (m, 2H), 7.58 (t, *J* = 7.4 Hz, 2H), 7.54–7.45 (m, 2H), 6.66 (d, *J* = 7.4 Hz, 1H), 6.62 (d, *J* = 8.3 Hz, 1H), 3.38 (s, 2H), 1.59 (s, 3H). ¹³C-NMR (101 MHz, CDCl₃) δ 153.61 (1C), 153.16 (1C), 150.50 (1C), 150.35 (1C), 147.95 (1C), 147.29 (1C), 140.95 (1C), 139.60 (1C), 133.80 (1C), 132.65 (1C), 131.19 (1C), 129.32 (2C), 127.20 (1C), 126.88 (1C), 124.19 (1C), 123.65 (1C), 123.43 (2C), 119.91 (1C), 116.90 (1C), 113.72 (1C), 112.75 (1C), 112.28 (1C), 107.60 (1C), 106.29 (1C), 67.38 (1C), 67.28 (1C), 51.05 (1C).

Synthesis of SBB-N₃

4-Dimethylaminopyridine (20 mg, 0.16 mmol) and *N,N'*-dicyclohexylcarbodiimide (110 mg, 0.5 mmol) were dissolved in anhydrous CH₂Cl₂ (10 mL) under an inert atmosphere. The mixture was stirred for 30 min and then 2-azidoacetic acid (30 μL, 0.4 mmol) was added. Compound **3** (0.220 mg, 0.45 mmol) was dissolved in CH₂Cl₂ under inert conditions and was then added dropwise to the 2-azidoacetic acid solution. The resulting mixture was stirred for 2 days. The solvent was removed under vacuum and the crude was purified with reverse phase column using CH₃OH as eluent. The product (**SBB-N₃**) was obtained as a purple solid (yield 41%). ¹H-NMR (400 MHz, CDCl₃) δ 9.15–9.09 (m, 1H), 9.07–9.01 (m, 1H), 8.46 (d, *J* = 8.0 Hz, 1H), 8.15 (d, *J* = 8.3 Hz, 1H), 8.12–8.06 (m, 2H), 8.01 (dd, *J* = 20.2, 8.4 Hz, 2H), 7.76–7.70 (m, 2H), 7.58 (t, *J* = 7.4 Hz, 2H), 7.54–7.45 (m, 2H), 6.65 (d, *J* = 6.9 Hz, 1H), 6.61 (d, *J* = 8.4 Hz, 1H), 4.07 (d, *J* = 6.9 Hz, 2H), 3.68 (s, 2H), 1.58 (d, *J* = 7.7 Hz, 3H). ¹³C-NMR (101 MHz, CDCl₃) δ 153.59 (1C), 150.49 (1C), 147.94 (1C), 144.46 (1C), 140.93 (1C), 139.60 (1C), 133.79 (1C), 132.64 (1C), 132.14 (1C), 131.19 (1C), 129.32 (2C), 127.20 (1C), 126.88 (1C), 124.19 (1C), 123.65 (1C), 123.42 (2C), 116.88 (2C), 113.70 (1C), 112.74 (2C), 112.27 (2C), 107.59 (1C), 106.28 (1C), 67.37 (1C), 67.25 (1C), 51.05 (1C), 24.84 (1C).

Synthesis of BODIPY

Fmoc-Trp-BODIPY (100 mg, 0.13 mmol), 1,1,3,3-tetramethyl-2-[2-oxopyridin-1(2H)-yl]isouronium hexafluorophosphate (189 mg, 0.013 mmol) and *N,N*-diisopropylethylamine (25.5 μL,

0.15 mmol) were introduced in a two-neck flask and dissolved with anhydrous DMF (5 mL) under an inert atmosphere. The obtained mixture was stirred at room temperature for 15 min. Then, *N*-[(1*R*,8*S*,9*S*)-bicyclo[6.1.0]non-4-yn-9-ylmethyloxycarbonyl]-1,8-diamino-3,6-dioxaoctane (50 mg, 0.15 mmol) was dissolved in anhydrous DMF (5 mL) and was added dropwise to the Fmoc-Trp-BODIPY solution. The reaction was stirred at room temperature for 24 h and the solvent was removed under reduce pressure. The crude was purified by silica column using ethyl acetate : hexane (1 : 1 v/v) as eluent. The final product (**BODIPY**) was obtained as a red solid (yield 89%). ¹H-NMR (400 MHz, dimethylsulfoxide) δ 11.28 (s, 1H), 7.91 (d, *J* = 8.3 Hz, 1H), 7.88 (d, *J* = 7.2 Hz, 2H), 7.80 (m, 1H), 7.68 (t, *J* = 7.4 Hz, 4H), 7.59–7.54 (m, 1H), 7.41 (dd, *J* = 11.5, 7.4 Hz, 2H), 7.36 (d, *J* = 7.6 Hz, 1H), 7.31 (d, *J* = 8.3 Hz, 2H), 7.27 (m, 1H), 7.07 (dd, *J* = 15.6, 7.6 Hz, 2H), 6.95 (dd, *J* = 14.4, 7.4 Hz, 1H), 4.39–4.31 (m, 1H), 4.18–4.07 (m, 2H), 4.06–3.98 (m, 3H), 3.17 (d, *J* = 5.3 Hz, 1H), 3.10–3.01 (m, 5H), 2.69 (s, 2H), 2.67 (dt, *J* = 3.6, 1.8 Hz, 2H), 2.45 (ws, 4H), 2.37 (ws, 2H), 2.33 (dt, *J* = 3.7, 1.8 Hz, 1H), 2.25–2.12 (m, 4H), 1.99 (s, 1H), 1.44 (m, *J* = 5.2 Hz, 6H), 1.26 (s, 1H), 1.23 (ws, 1H), 1.17 (t, *J* = 7.1 Hz, 1H), 1.09 (s, 1H), 1.02 (d, *J* = 11.4 Hz, 1H), 0.83 (ddt, *J* = 17.3, 15.0, 7.4 Hz, 4H). ¹³C-NMR (101 MHz, CDCl₃) δ 207.16 (1C), 171.11 (2C), 157.18 (1C), 155.71 (2C), 143.99 (1C), 143.84 (1C), 143.23 (1C), 143.12 (1C), 141.35 (1C), 141.07 (1C), 136.27 (1C), 135.83 (1C), 134.76 (1C), 133.82 (1C), 131.49 (1C), 131.41 (1C), 130.09 (1C), 129.01 (1C), 128.62 (1C), 128.41 (1C), 127.79 (1C), 127.33 (1C), 127.26 (1C), 127.16 (1C), 126.81 (1C), 125.68 (1C), 125.23 (1C), 122.98 (1C), 121.39 (1C), 120.22 (1C), 120.04 (1C), 119.51 (1C), 118.04 (1C), 111.22 (1C), 110.70 (1C), 108.29 (1C), 98.87 (2C), 70.09 (1C), 70.01 (1C), 69.30 (1C), 67.11 (1C), 63.02 (1C), 55.61 (1C), 47.20 (1C), 40.69 (1C), 39.34 (1C), 38.69 (1C), 30.99 (1C), 29.77 (1C), 29.33 (1C), 29.08 (1C), 28.55 (1C), 24.78 (1C), 23.52 (1C), 21.47 (1C), 20.18 (1C), 17.79 (1C), 14.67 (1C), 14.64 (1C).

Monitoring of the click reaction by HPLC-MS

To confirm the formation of the Click reaction product, HPLC-MS measurements were carried out. For this purpose, **SBB-N₃** (2 mg, 3.6 μmol) and **BODIPY** (2 mg, 1.9 μmol) reagents were dissolved in 360 and 190 μL of dimethylsulfoxide, respectively, to obtain 10 mM stock solutions of both compounds. Next, 20 μL of stock solutions of **SBB-N₃** and **BODIPY** were diluted in 1 mL of distilled water, obtaining 200 μM aqueous solutions (dimethylsulfoxide: water, 2 : 98 v/v) of **SBB-N₃** and **BODIPY**. In addition, 10 μL of pure reagents aqueous solution (200 μM) was dissolved in 500 μL of methanol to obtain pure reagent solution that was injected into the HPLC-MS. To confirm the formation of click reaction product, an aqueous solution of both reagents was heated at 37 °C for 1 h, and 1 mL of the **SBB-N₃** solution (200 μM) was mixed with 1 mL of the **BODIPY** solution (200 μM), with the reaction being maintained at 37 °C for 5 h. Next, 20 μL of crude

reaction was dissolved in 500 μL of methanol. Pure reagent final solutions (4 μM) and reaction crude (4 μM) were directly injected into the HPLC-MS using a gradient eluent method from H₂O-acetonitrile (90 : 10 v/v) to H₂O-acetonitrile (90 : 10 v/v) at 10 min with a flow rate 0.4 mL·min⁻¹. Ultraviolet spectra were recorded via an Agilent 1620 Infinity II photodiode array at 500 nm (Fig. S6). MS chromatograms were recorded with an Agilent Ultivo mass spectrometer equipped with a triple Q-TOF detector using the selected ion monitoring function.

Monitoring of the click reaction by ATR-FTIR

To obtain ATR-FTIR spectra, 5 μL of the 10 mM solutions of **SBB-N₃** and **BODIPY** were diluted in 5 mL of distilled water, obtaining aqueous solutions (dimethylsulfoxide : water, 1 : 99 v/v) of 10 μM for both products. Next, 5 mL of the **BODIPY** solution (10 μM, 50 μmol) was mixed with 5 mL of the **SBB-N₃** solution (10 μM, 50 μmol) and the reaction was maintained for 2 h at 37 °C. Finally, the crude reaction was dried. Solid obtained and pure reagents were analyzed in a Nicolet 6700 instrument (Thermo Scientific) in the range 4000–400 cm⁻¹, comparing the obtained spectrum with that of the starting reagents.

Cell lines

Human melanoma SK-Mel-103 cells, human triple-negative breast cancer MDA-MB-231 cells and human lung fibroblasts WI-38 cells were obtained from the ATCC (Manassas, VA, USA). Cells were maintained in DMEM, supplemented with 10% fetal bovine serum, and incubated in 20% O₂ and 5% CO₂ at 37 °C. Cells were routinely tested for contamination using the *Mycoplasma* tissue culture NI (MTC-NI) Rapid Detection System (Gen-Probe, San Diego, CA, USA). For senescence induction, cells were supplemented for 1 week with media containing 5 μM palbociclib.

In vitro cell viability assays

Proliferative and senescent SK-MEL-103, MDA-MB-231 and WI-38 cells, respectively, were used for cell viability assays. Control (proliferative) and senescent cells were placed in flat-bottom-clear 96-well plates at a density of 6000 and 4000 cells per well, respectively. The following day, cells were treated with serial dilutions of **BODIPY**, **SBB-N₃** or combined **SBB-N₃ + BODIPY**. Viability was assessed 48 h later with a CellTiter-GLO Luminescent Cell Viability Assay (Promega) (Fig. S7). Raw data were obtained by measuring luminescence in a VICTOR Multilabel Plate Reader (PerkinElmer). To calculate the percentage of viability, in each assay each value was normalized to the average of the respective control group of proliferative

(untreated cells) or senescent cells and finally multiply by 100. The results are expressed as the mean \pm SD of three independent studies ($n = 3$). Statistical analysis was performed by applying two-way analysis of variance with multiple comparisons using PRISM (GraphPad Software Inc., San Diego, CA, USA).

β -galactosidase activity and lipofuscin staining

The induction of senescence after palbociclib treatment in SK-Mel-103 cells was confirmed using a Senescence β -Galactosidase Staining Kit (#9860; Cell Signaling, Danvers, MA, USA) in accordance with the manufacturer's instructions. In parallel, cells were treated with the Sudan Black B derivative **SBB-N₃** ($3.2 \mu\text{g}\cdot\text{mL}^{-1}$) for 2 h to correlate cellular senescence lipofuscin staining. Cells were observed using optical microscopy.

Flow cytometry studies

Control and senescent cells were placed in flat-bottom-clear 24-well plates at a density of 30 000 cells per well. Cells were treated with **SBB-N₃** solution ($3.2 \mu\text{g}\cdot\text{mL}^{-1}$) for 2 h. Then cells were washed with DMEM (3 \times) and incubated for 1 h with serial dilutions of **BODIPY** from 5 to 15 μM . Cells were washed again with DMEM (2 \times) and PBS (1 \times), trypsinized and detached from plates. Then, the cells were analyzed by flow cytometry and data were acquired using an FC500 MPL Flow Cytometer (Beckman, Brea, CA, USA) (Fig. S8).

Confocal microscopy assays

Control and senescent cells were seeded in a 96-well Black OptiPlate (PerkinElmer) at a concentration of 5000 cells per well for SK-Mel-103, MDA-MB-231 and WI-38 cells. After 24 h, cells were treated with **SBB-N₃** solution ($3.2 \mu\text{g}\cdot\text{mL}^{-1}$) for 2 h. Next, the cells were washed with DMEM and then **BODIPY** at 5 μM was added for 1 h. Finally, the cells were washed with PBS and then Hoechst 33348 ($2 \mu\text{g}\cdot\text{mL}^{-1}$) was added for nuclei staining. Confocal fluorescence images were taken on a TCS SP8 AOBS using 488 nm as excitation wavelength. The laser intensity was set up under conditions in which the autofluorescence of the senescent cells did not interfere with the fluorescence of the compound. Images were obtained at 20 \times magnification, and the fluorescence intensity was analyzed cell by cell, from different fields (randomly selected) conformed by 50–100 cells in each one using IMAGEJ. To calculate the percentage of fluorescence intensity, in each assay, we normalized each value (proliferative and senescent) to the average of the higher fluorescence signal and finally multiplied by 100. The results are expressed as the mean \pm SD of three independent studies ($n = 3$). To obtain images at high magnification (63 \times), proliferative and senescent cells were seeded

at a concentration of 250 000 cells per well for SK-Mel-103, MDA-MB-231 and WI-38 cells. After 24 h, cells were treated with **SBB-N₃** solution ($3.2 \mu\text{g}\cdot\text{mL}^{-1}$) for 2 h. Next, the cells were washed with DMEM and then **BODIPY** at 5 μM was added for 1 h. Finally, cells were washed with PBS, coverslips were mounted and Hoechst 33348 ($2 \mu\text{g}\cdot\text{mL}^{-1}$) was added for nuclei staining. Confocal fluorescence images were taken on a TCS SP8 AOBS. The results showed representative images from three independent studies ($n = 3$).

Acknowledgements

RM laboratory members are grateful for financial support from the FEDER foundation of European Union (IDIFEDER/2021/044), the Spanish Government (projects RTI2018-100910-B-C41 and RTI2018-101599-B-C22) and the Generalitat Valenciana (project PROMETEO 2018/024). BL-T and AG-F acknowledge their current Margarita Salas postdoctoral fellowship from UPV-MIU and 'Next Generation EU' program. JF-B is grateful for his Sara Borrell postdoctoral fellowship (CD19/00038).

Conflicts of interest

The authors declare that they have no conflicts of interest.

Author contributions

BL-T, JFB, AG-F, FSG and RM-M conceived and designed the research. BL-T and JFB synthesized and characterized all organic molecules. JFB performed the characterization studies. BL-T carried out the cellular studies with the SK-MEL-103 cell line. AGF performed cellular assays with MDA-MB-231 and WI-38 cells. BL-T, JFB and AGF collected the data, conceived and designed the analysis, and contributed to the discussion of the results. BL-T, JFB and AGF wrote the manuscript. FS and RM-M supervised the data analysis, contributed to discussion and revised the manuscript.

Peer review

The peer review history for this article is available at <https://publons.com/publon/10.1111/febs.16477>.

References

- 1 Muñoz-Espín D, Serrano M. Cellular senescence: from physiology to pathology. *Nat Rev Mol Cell Biol.* 2014;15:482–96.

- 2 Mosteiro L, Pantoja C, de Martino A, Serrano M. Senescence promotes in vivo reprogramming through p16 INK4a and IL-6. *Aging Cell*. 2018;**17**:e12711.
- 3 Ritschka B, Storer M, Mas A, Heinzmann F, Ortells MC, Morton JP, et al. The senescence-associated secretory phenotype induces cellular plasticity and tissue regeneration. *Genes Dev*. 2017;**31**:172–83.
- 4 McHugh D, Gil JJ. Senescence and aging: causes, consequences, and therapeutic avenues. *Cell Biol*. 2018;**217**:65–77.
- 5 Lozano-Torres B, Blandez JF, Galiana I, Lopez-Dominguez JA, Rovira M, Paez-Ribes M, et al. A Two-Photon probe based on naphthalimide-styrene fluorophore for the in vivo tracking of cellular senescence. *Anal Chem*. 2021;**93**:3052–60.
- 6 Lozano-Torres B, Estepa-Fernandez A, Rovira M, Orzáez M, Serrano M, Martínez-Mañez R, et al. The chemistry of senescence. *Nat Rev Chem*. 2019;**3**:426–41.
- 7 Muñoz-Espín D, Rovira M, Galiana I, Giménez C, Lozano-Torres B, Paez-Ribes M, et al. A versatile drug delivery system targeting senescent cells. *EMBO Mol Med*. 2018;**10**:e9355.
- 8 González-Gualda E, Paez-Ribes M, Lozano-Torres B, Macías D, Wilson JR, González-López C, et al. Galacto-conjugation of Navitoclax as an efficient strategy to increase senolytic specificity and reduce platelet toxicity. *Aging Cell*. 2020;**19**:e13142.
- 9 Galiana I, Lozano-Torres B, Sancho M, Alfonso M, Bernardos A, Bisbal V, et al. Preclinical antitumor efficacy of senescence-inducing chemotherapy combined with a nanoSenolytic. *J Control Release*. 2020;**323**: 624–34.
- 10 Alejandra Estepa-Fernández A, Alfonso M, Morellá-Aucejo A, García-Fernández A, Lérida-Viso A, Lozano-Torres B, et al. Senolysis reduces senescence in veins and cancer cell migration. *Adv Ther*. 2021;**4**:2100149.
- 11 Baker DJ, Childs BG, Durik M, Wijers ME, Sieben CJ, Zhong J, et al. Naturally occurring p16(Ink4a)-positive cells shorten healthy lifespan. *Nature*. 2016;**530**:184–9.
- 12 Baker DJ, Wijshake T, Tchkonja T, LeBrasseur NK, Childs BG, van de Sluis B, et al. Clearance of p16Ink4a-positive senescent cells delays aging-associated disorders. *Nature*. 2011;**479**:232–6.
- 13 Lozano-Torres B, Galiana I, Rovira M, Garrido E, Chaib S, Bernardos A, et al. An OFF–ON two-photon fluorescent probe for tracking cell senescence in vivo. *J Am Chem Soc*. 2017;**139**:8808–11.
- 14 Lozano-Torres B, Blandez JF, Galiana I, García-Fernández A, Alfonso M, Marcos MD, et al. Real-Time in vivo detection of cellular senescence through the controlled release of the NIR fluorescent dye Nile Blue. *Angew Chem Int Ed*. 2020;**59**:15152–6.
- 15 Lozano-Torres B, Blandez JF, Sancenón F, Martínez-Mañez R. Chromo-fluorogenic probes for β -galactosidase detection. *Anal Bioanal Chem*. 2021;**413**:2361–88.
- 16 Lozano-Torres B, Blandez JF, Sancenón F, Martínez-Mañez R. Novel probes and carriers to target senescent cells. In: Muñoz-Espín D, Demaria M, editors. *Senolytics in disease, ageing and longevity*. Cham, Switzerland: Springer International Publishing; 2020. p. 163–80.
- 17 Asanuma D, Sakabe M, Kamiya M, Yamamoto K, Hiratake J, Ogawa M, et al. Sensitive β -galactosidase-targeting fluorescence probe for visualizing small peritoneal metastatic tumors in vivo. *Nat Commun*. 2015;**6**:6463–70.
- 18 Jiang G, Zeng G, Zhu W, Li Y, Dong X, Zhang G, et al. A selective and light-up fluorescent probe for β -galactosidase activity detection and imaging in living cells based on an AIE tetraphenylethylene derivative. *Chem Commun*. 2017;**53**:4505–8.
- 19 Terman A, Brunk UT. Lipofuscin. *Int J Biochem Cell Biol*. 2004;**36**:1400–4.
- 20 Georgakopoulou EA, Tsimaratou K, Evangelou K, Fernandez Marcos PJ, Zoumpourlis V, Trougakos IP, et al. Specific lipofuscin staining as a novel biomarker to detect replicative and stress-induced senescence. A method applicable in cryo-preserved and archival tissues. *Aging*. 2013;**5**:1–14.
- 21 Gatenby JB, Moussa TA. The Sudan black B technique in cytology. *J R Microsc Soc*. 1949;**69**:72–5.
- 22 Rasmussen GL. A method of staining the statoacoustic nerve in bulk with Sudan black B. *Anat Rec*. 1961;**139**:465–9.
- 23 Jung T, Hohn A, Grune T. Lipofuscin: detection and quantification by microscopic techniques. *Methods Mol Biol*. 2010;**594**:173–93.
- 24 Evangelou K, Lougiakis N, Rizou SV, Kotsinas A, Kletsas D, Muñoz-Espín D, et al. Robust, universal biomarker assay to detect senescent cells in biological specimens. *Aging Cell*. 2017;**16**:192–7.
- 25 Devaraj NK. The future of bioorthogonal chemistry. *ACS Cent Sci*. 2018;**4**:952–9.
- 26 Hein CD, Liu XM, Wang Dong. Click Chemistry, a powerful tool for pharmaceutical sciences. *Pharm Res*. 2008;**25**:2216–30.
- 27 Devaraj NK, Finn MG. Introduction: click chemistry. *Chem Rev*. 2021;**121**:6697–8.
- 28 Scinto SL, Bilodeau DA, Hincapie R, Lee W, Nguyen SS, Xu M, et al. Bioorthogonal chemistry. *Nat Rev Dis Primers*. 2021;**1**:30–53.
- 29 Nwe K, Brechbie MW. Growing applications of “Click Chemistry” for bioconjugation in contemporary biomedical research. *Cancer Biother Radiopharm*. 2009;**24**:289–302.

- 30 Kolb HC, Sharpless KB. The growing impact of click chemistry on drug discovery. *Drug Discov Today*. 2003;**8**:1128–37.
- 31 Bock VD, Hiemstra H, van Maarseveen JH. CuI-Catalyzed Alkyne-Azide “Click” cycloadditions from a mechanistic and synthetic perspective. *Eur J Org Chem*. 2005;**1**:51–68.
- 32 Binder WH, Kluger C. Azide/Alkyne-“click” reactions: applications in material science and organic synthesis. *Curr Org Chem*. 2006;**10**:1791–815.
- 33 Binder WH, Sachsenhofer R. ‘Click’ chemistry in polymer and materials science. *Macromol Rapid Commun*. 2007;**28**:15–54.
- 34 Moorhouse AD, Moses JE. Click chemistry and medicinal chemistry: a case of “Cyclo-Addiction”. *Chem Med Chem*. 2008;**3**:715–23.
- 35 Jewetta JC, Bertozz CR. Cu-free click cycloaddition reactions in chemical biology. *Chem Soc Rev*. 2010;**39**:1272–9.
- 36 McKay CS, Finn MG. Click chemistry in complex mixtures: bioorthogonal bioconjugation. *Chem Biol*. 2014;**21**:1075–101.
- 37 Kim E, Koo H. Biomedical applications of copper-free click chemistry: in vitro, in vivo, and ex vivo. *Chem Sci*. 2019;**10**:7835–51.

Supporting information

Additional supporting information may be found online in the Supporting Information section at the end of the article.

Fig. S1. $^1\text{H-NMR}$ and $^{13}\text{C-NMR}$ of compound **1**.

Fig. S2. $^1\text{H-NMR}$ and $^{13}\text{C-NMR}$ of compound **2**.

Fig. S3. $^1\text{H-NMR}$ and $^{13}\text{C-NMR}$ of compound **3**.

Fig. S4. $^1\text{H-NMR}$ and $^{13}\text{C-NMR}$ of compound **SBB-N₃**.

Fig. S5. $^1\text{H-NMR}$ and $^{13}\text{C-NMR}$ of compound **BOD-IPY**.

Fig. S6. Monitoring of the click reaction by HPLC-MS.

Fig. S7. *In vitro* cell viability assay.

Fig. S8. Flow cytometry studies.

Fig. S9. Confocal imaging studies of control and palbociclib-treated SK-Mel-103 cells.

Fig. S10. Confocal imaging studies of control and palbociclib-treated MDA-MB-231 cells.

Fig. S11. Confocal imaging studies of control and palbociclib-treated WI-38 fibroblasts.